nature nanotechnology

ARTICLES

PUBLISHED ONLINE: 17 OCTOBER 2016 | DOI: 10.1038/NNANO.2016.178

A dressed spin qubit in silicon

Arne Laucht[1]*, Rachpon Kalra[1], Stephanie Simmons[1], Juan P. Dehollain[1], Juha T. Muhonen[1], Fahd A. Mohiyaddin[1], Solomon Freer[1], Fay E. Hudson[1], Kohei M. Itoh[2], David N. Jamieson[3], Jeffrey C. McCallum[3], Andrew S. Dzurak[1] and A. Morello[1]*

Coherent dressing of a quantum two-level system provides access to a new quantum system with improved properties—a different and easily tunable level splitting, faster control and longer coherence times. In our work we investigate the properties of the dressed, donor-bound electron spin in silicon, and assess its potential as a quantum bit in scalable architectures. The two dressed spin-polariton levels constitute a quantum bit that can be coherently driven with an oscillating magnetic field, an oscillating electric field, frequency modulation of the driving field or a simple detuning pulse. We measure coherence times of $T_{2\rho}^{\star}$ = 2.4 ms and $T_{2\rho}^{\mathrm{Hahn}}$ = 9 ms, one order of magnitude longer than those of the undressed spin. Furthermore, the use of the dressed states enables coherent coupling of the solid-state spins to electric fields and mechanical oscillations.

Coherent dressing of a quantum two-level system has been demonstrated on a variety of systems, including atoms[1], self-assembled quantum dots[2], superconducting quantum bits[3] and nitrogen-vacancy (NV) centres in diamond[4]. In this context 'dressing' means that an electromagnetic driving field coherently interacts with the quantum system, so that the eigenstates of the driven system are the entangled states of the photons and the quantum system. For the case of a single spin in a static magnetic field B_0 that is driven with an oscillating magnetic field B_1, this means that the eigenstates are no longer the spin-up and spin-down states, but the symmetric and antisymmetric superpositions of these states with the driving field (Fig. 1b).

The dressed system possesses a level splitting proportional to the driving strength, and can therefore be modified dynamically and tuned to be in resonance with other quantum systems[4–6]. Furthermore, the continuous driving decouples the spin from background magnetic field noise. Even in highly coherent systems such as trapped atoms, coherence times can be improved by two orders of magnitude by dressing the states[7]. Finally, the change in quantization axis unlocks new ways of operating on a dressed qubit. A dressed qubit can be controlled by changes in the bare spin Larmor frequency, which allows manipulation using electric fields and strain via the hyperfine coupling in donor systems[8,9]. This opens up the possibility of coupling spins to the motion of a mechanical oscillator when the transition frequency between dressed states becomes comparable to the oscillator's frequency[10,11].

As a result of these benefits, it has been proposed that dressed states be used for quantum gates and memories for quantum computing[7,12,13]. In these proposals, the focus was on optically dressed qubits in trapped atomic ions, because dressing a qubit fundamentally requires a high ratio between the driving field and the intrinsic resonance linewidth, most easily achieved in optics and trapped ions. Here we demonstrate a microwave (MW)-dressed spin qubit in the solid state, using a highly coherent ^{31}P-donor-bound electron in silicon[14]. We demonstrate that the use of dressed states, compared with that of bare spin states, has several advantages for quantum computation.

The ^{31}P donor in silicon constitutes a natural two-qubit system, in which both the electron (indicated with $|\downarrow\rangle$ or $|\uparrow\rangle$) and the nuclear ($|\Downarrow\rangle$ or $|\Uparrow\rangle$) spin states can be controlled coherently by a magnetic field B_1 oscillating at specific electron-spin resonance (ESR) and nuclear magnetic resonance frequencies. Figure 1a shows a device similar to the one measured. It consists of a single ^{31}P donor in an isotopically purified ^{28}Si epilayer[15], implanted[16] next to the island of a single-electron transistor (SET). The SET is formed by biasing a set of electrostatic gates (yellow), whereas donor gates (pink) are used to tune the electrochemical potential μ of the donor with respect to that of the SET island. The device is cooled down to $T_{\mathrm{electron}} \approx 100$ mK, and subjected to a static magnetic field $B_0 = 1.55$ T. High-fidelity, single-shot electron-spin readout as well as initialization of the donor electron spin into the $|\downarrow\rangle$ state is achieved via spin-dependent tunnelling of the electron to the SET island[17,18]. Coherent spin control is achieved with an oscillating magnetic field B_1 delivered to the donor through an on-chip, broadband, nanoscale antenna[19] (blue in Fig. 1a).

Dressing the electron spin

Figure 1b shows the energy-level diagram of the electron-spin subsystem. Naturally, we would draw the energy levels in the $|\uparrow\rangle$—$|\downarrow\rangle$ basis, which corresponds to the spin picture, with electron-spin transition frequency ν_e. Alternatively, we can draw them in the dressed $|N+1\rangle$—$|N\rangle$ basis, where N is the total number of excitations in the system. The state $|N\rangle$ then consists of the two degenerate states $|\downarrow, n\rangle$ and $|\uparrow, n-1\rangle$, where n is the number of resonant photons in the driving field. For a non-zero spin–photon coupling, the dressed levels are split into the entangled $|+, N\rangle = (1/\sqrt{2})(|\downarrow, n\rangle + |\uparrow, n-1\rangle)$ and $|-, N\rangle = (1/\sqrt{2})(|\downarrow, n\rangle - |\uparrow, n-1\rangle)$ states, which differ in energy by the Rabi frequency $\Omega_R = (1/2)\gamma_e B_1$ where $\gamma_e = 28$ GHz/T is the gyromagnetic ratio of the electron and B_1 is the amplitude of the oscillating driving field.

We can define the dressed spin states as the basis states of a new qubit, the dressed qubit. Here the states $|-\rangle$ and $|+\rangle$ act as the computational basis states. We have omitted N, the number of excitations in the system, as the electron is dressed by a classical driving field, in

[1]Centre for Quantum Computation and Communication Technology, School of Electrical Engineering and Telecommunications, UNSW Australia, Sydney, New South Wales 2052, Australia. [2]School of Fundamental Science and Technology, Keio University, 3-14-1 Hiyoshi, Kanagawa 223-8522, Japan. [3]Centre for Quantum Computation and Communication Technology, School of Physics, University of Melbourne, Melbourne, Victoria 3010, Australia.
*e-mail: a.laucht@unsw.edu.au; a.morello@unsw.edu.au

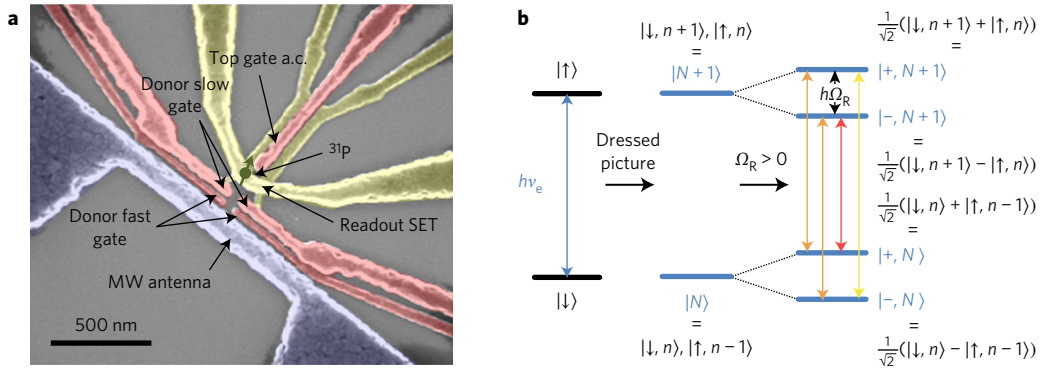

Figure 1 | Sample design and energy level diagram. a, Scanning electron microscope image of a device similar to the one used for measurements. Highlighted are the positions of the ^{31}P donor, the donor gates (pink), the MW antenna (blue) and the SET for spin readout (yellow). **b**, Energy-level diagram of the electron-spin subsystem in the spin picture and the dressed picture (see the text).

which the number of photons n is very large and its exact value is unimportant. We do, however, need to take into account the magnitude of B_1, which defines the electron Rabi frequency Ω_R and therefore the splitting between the $|-\rangle$ and $|+\rangle$ states.

There are two ways to demonstrate the creation of dressed states. The first is by performing coherent Rabi oscillations, which has been demonstrated on electron and nuclear spins in many material systems for ensembles[20,21] and single spins[22–26]. The second is by measuring the Mollow triplet[1]. This, however, is more difficult as the Mollow spectrum is usually measured in transmission/absorption[2,3,27] or fluorescence/scattering[1,28,29] and requires a very sensitive optical detector and outstanding background suppression. Here we implement a novel way to measure the Mollow spectrum, based on our high-fidelity control and spin readout.

After initializing the donor electron in the $|\downarrow\rangle$ state, we apply a resonant, high-power MW pulse (pump pulse) which creates the dressed states with a splitting equal to the Rabi frequency Ω_{pump}. We choose the length of the pulse to be $m\pi$, where m is an integer, which makes the effect of this pulse traceable. For the measurements in Fig. 2, we use a rotation angle of 21π, which rotates the spin to the $|\uparrow\rangle$ state. Simultaneously to the pump pulse, a low-power MW pulse (probe pulse) of the same length is applied to probe the response of the driven spin to different frequencies. The probe pulse on its own would lead to a $\sim\pi$ rotation when in resonance. However, in combination with the pump pulse, it will drive the four different transitions of the Mollow triplet, indicated in red, orange and yellow in Fig. 1b.

In Fig. 2, we plot the spectra obtained by scanning the probe frequency over the resonance for different MW powers. The pump power was increased from $P_{pump} = -4$ dBm (at the source) to $P_{pump} = +8$ dBm, and the probe power was always kept 26 dB lower, that is, $P_{probe} = P_{pump} - 26$ dB. The spectra consist of a larger peak in the middle and two smaller peaks split off by the Rabi frequency Ω_{pump}, in agreement with the Mollow triplet. When increasing the MW power, this splitting increases because of the stronger drive, as expected. At the same time, the width of the peaks increases because a higher probe power is necessary to keep the power ratio constant. The insets of Fig. 2 show standard Rabi oscillation experiments for the same MW powers. The extracted Rabi frequencies are in excellent agreement with the peak splitting of the Mollow triplet. In Supplementary Section 3 we show additional data for different pulse lengths (Supplementary Fig. 1) and P_{probe}/P_{pump} ratios (Supplementary Fig. 2).

Dressed qubit initialization and readout

All of our measurements are based on the initialization of the electron spin in the $|\downarrow\rangle$ state and readout of the $|\uparrow\rangle$ state via spin-dependent tunnelling to the SET island[18]. To work with the dressed qubit, we need to convert the electron $|\downarrow\rangle$, $|\uparrow\rangle$ states into the dressed qubit $|-\rangle$, $|+\rangle$ states and vice versa. This can be done in two ways. The first is to use resonant $\pi/2$ pulses along the $-y'$-axis in the frame of the MW source (Supplementary Fig. 4a), which will convert $|\downarrow\rangle$ to $|+\rangle$ for the initialization, and $|+\rangle$ to $|\uparrow\rangle$ for the readout. Between initialization and readout, the spin needs to be resonantly driven about the x'-axis to keep it spin-locked in the dressed picture[20]. The second is to start with an off-resonant MW driving field along the x'-axis and adiabatically reduce the detuning $\Delta\nu = \nu_e - \nu_{MW}$ between the ESR transition frequency ν_e and the MW frequency ν_{MW} to zero. This will convert $|\downarrow\rangle$ to $|-\rangle$ when reducing $\Delta\nu$ for initialization, and $|+\rangle$ to $|\uparrow\rangle$ when increasing $\Delta\nu$ for readout (also see Fig. 3g).

Dressed qubit control

The Hamiltonian H of the system is given in the basis of the spin states $|\downarrow\rangle$ and $|\uparrow\rangle$ by:

$$H = \frac{1}{2}h\gamma_e(B_0\sigma_z + B_1\cos(2\pi\nu_{MW}t)\sigma_x) \quad (1)$$

in the lab frame, and by

$$H_{rot} = \frac{1}{2}h(\Delta\nu\sigma_z + \Omega_R\sigma_x) \quad (2)$$

in the rotating frame. We can change our basis to make the eigenstates of the driven system ($|+\rangle = (1/\sqrt{2})(|\downarrow\rangle + |\uparrow\rangle)$ and $|-\rangle = (1/\sqrt{2})(|\downarrow\rangle - |\uparrow\rangle)$) the basis states of our Hilbert space and we obtain the Hamiltonian in the dressed basis

$$H_\rho = \frac{1}{2}h(\Omega_R\sigma_z + \Delta\nu\sigma_x) \quad (3)$$

where the quantization is determined by Ω_R and the coupling term by $\Delta\nu$. This offers a number of different methods to control the dressed qubit coherently. In the following we introduce four different methods based on (1) magnetic resonance, modulating $\Delta\nu$ at frequency Ω_R via (2) the Stark shift of ν_e (ref. 8) or via (3) frequency modulation of ν_{MW} and (4) pulsing $\Delta\nu$ high by changing ν_{MW} for a short period of time.

Magnetic resonance. The first method to control the dressed qubit is to apply a radiofrequency (RF) field B_2 with frequency $\nu_{RF} = \Omega_R$ via the on-chip antenna. Here only the magnetic field component perpendicular to the quantization axis of the dressed qubit drives the transition[30], and the dressed qubit Rabi frequency is given by $\Omega_{R\rho} = \cos(\theta)(1/2)\gamma_e B_2$, where θ is the angle between the orientation of the external magnetic field B_0 and that of the oscillating RF field B_2. Simulations of the on-chip antenna[19] and the donor device[8] indicate $\theta \approx 88°$ at the donor location.

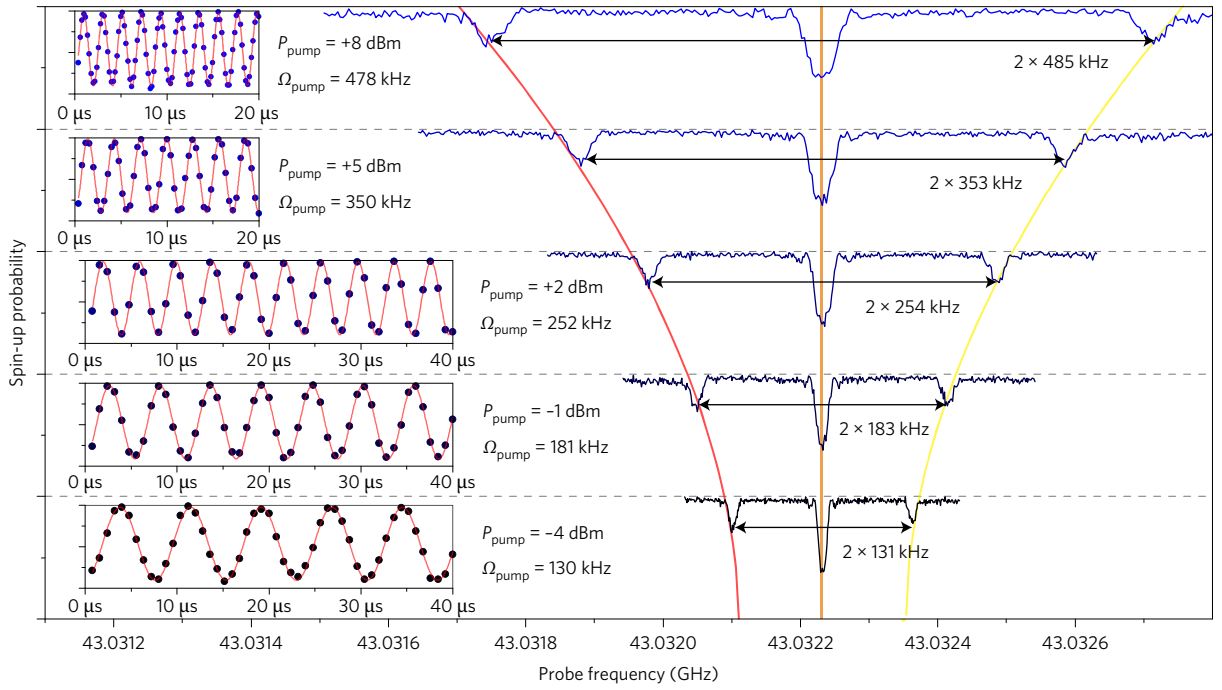

Figure 2 | Dressing the electron spin. Mollow spectra of the dressed electron spin for different MW powers obtained by measuring the spin-up probability after applying the MW pulses. Here a strong, resonant driving field P_{pump} is used to dress the spin state, whereas a weaker probe field $P_{probe} = P_{pump} - 26$ dB is scanned in frequency to record the Mollow triplet spectra. (The curves are shifted in frequency to compensate the slight drift of the background magnetic field B_0). The insets on the left show standard Rabi experiments for the same MW powers (the vertical scale is the electron spin-up probability from 0 to 1) with Rabi frequencies that match the splitting between the peaks of the Mollow triplet. Here the dots correspond to the experimental result, and the red lines are fits to a sinusoid.

We measure the spectral response of the dressed qubit by scanning ν_{RF} over the frequency range around Ω_R, and plot the spectra in Fig. 3a. With $\nu_{RF} = \Omega_R$ we can also measure coherent Rabi oscillations of the dressed qubit (Fig. 3b) with $\Omega_{R\rho} = 2.4$ kHz.

In principle, another way to use magnetic resonance would be to use a second MW field at ν_e along y', whose amplitude is modulated at Ω_R.

Electric resonance. In H_ρ (equation (3)), the off-diagonal terms (σ_x terms) directly depend on $\Delta\nu$. The electric field created by the gates can be used to induce a Stark shift of both the hyperfine coupling A between the electron and the nucleus, and the gyromagnetic ratio γ_e of the electron[8]. In Fig. 3c, we present the shift in resonance frequency ν_e for a d.c. voltage applied to two of the donor gates, and we extract a shift of $d\nu_e/dV = -167$ kHz V^{-1}. We can exploit the Stark shift to modulate $\Delta\nu$ at the dressed qubit's resonance frequency Ω_R to drive electrically the Rabi oscillations of the dressed qubit. As this control method makes use of a local electric gate to modulate ν_e, it is immediately compatible with scalable quantum computing architectures that comprise a global, always-on driving field (see Scalability below). Rabi oscillations (Fig. 3d) obtained with electric resonance show a frequency of $\Omega_{R\rho} = 3.1$ kHz, in excellent agreement with our prediction (Supplementary Section 4).

Frequency modulation (FM) resonance. Alternatively to electrical modulation of $\Delta\nu$ via the Stark shift, we can also modulate $\Delta\nu$ by FM of ν_{MW}. The FM feature in our MW source provides a simpler way to implement this method experimentally, albeit with the lack of the scale-up potential provided by electric resonance (see above). This is because one has to keep track of the reference frequency that defines the rotating frame, given by ν_{MW}. Another advantage of FM control is the much larger achievable Rabi frequency. The effective driving strength is limited only by the FM depth of the source and can reach the regime in which the driving strength exceeds the qubit splitting, $\Omega_{R\rho} > \Omega_R$ (ref. 31).

In Fig. 3e,f we plot the dressed qubit Rabi chevron pattern and spectrum, respectively. For these measurements, the output of the RF source is connected directly to the FM input of the MW source. The modulation amplitude $\Delta\nu_{MW}$ can then be controlled by the power of the RF source and the FM depth of the MW source, and $\Omega_{R\rho} = (1/2)\Delta\nu_{MW}$.

Detuning pulse. The fourth method of dressed qubit control that we investigate is realized by pulsing the detuning $\Delta\nu$ from 0 to a finite value for the duration of the gate operation. For $\Delta\nu > \Omega_R$, the eigenstates are the spin basis states, and the dressed $|+\rangle$ state will nutate into the dressed $|-\rangle$ state performing a Rabi oscillation (Fig. 3g) with $\Omega_{R\rho} \approx \Delta\nu$. This control method is analogous to the control of the Cooper pair box[32] or the singlet–triplet qubit in semiconductor double quantum dots[33–35]. In principle, it is equivalent to pulse $\Delta\nu$ by tuning ν_e or ν_{MW}, albeit with the same limitations as for FM control (see above). For our current sample design we can only reach $\Delta\nu > \Omega_R$ by pulsing ν_{MW}, which is why we limit our experiments to this case. With an optimized gate layout we could also use local electric-field control in a scalable manner.

In Fig. 3h we plot the Rabi frequency of the dressed qubit $\Omega_{R\rho}$ as a function of $\Delta\nu_{MW}$ during the detuning pulse, with $\Omega_R = 460$ kHz. The dressed qubit Rabi frequency follows the dependence $\Omega_{R\rho} = \sqrt{\Delta\nu_{MW}^2 + \Omega_R^2}$ given by Rabi's formula perfectly (red line in Fig. 3h). The maximum $\Omega_{R\rho}$ shown here is 10 MHz, much larger than the dressed qubit's level-splitting Ω_R. Furthermore, $\Omega_{R\rho} = 10$ MHz corresponds to a gate-operation time one order of magnitude shorter than those normally obtained with pulsed ESR on the bare electron spin in our lab. For $\Delta\nu_{MW} \leq \Omega_R$, $\Omega_{R\rho}$ tends towards Ω_R and the amplitude of the Rabi oscillations decreases (also see Supplementary Section 5).

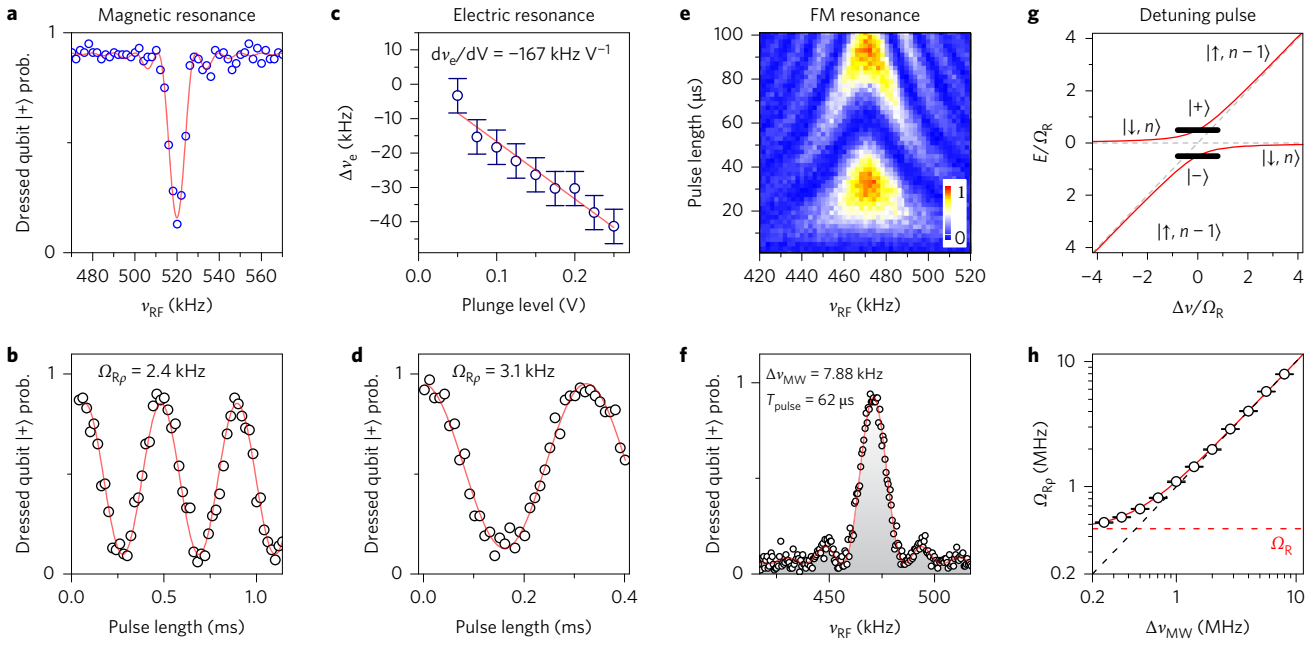

Figure 3 | Dressed qubit control. a,**b**, Dressed qubit spectrum (**a**) and Rabi oscillations (**b**) obtained via magnetic resonance. The circles are the experimental result, and the red lines are fits to Rabi's formula. **c**, Stark shift in resonance frequency ν_e of the electron-spin transition. **d**, Dressed qubit Rabi oscillations obtained via electric resonance. **e**,**f**, Dressed qubit chevron Rabi pattern (**e**) and spectrum obtained via FM resonance (**f**). The red line is a fit to Rabi's formula. **g**, Level scheme of the dressed qubit system as a function of detuning $\Delta\nu = \nu_e - \nu_{MW}$. **h**, Dressed qubit Rabi frequency as a function of $\Delta\nu_{MW}$ during the detuning pulse.

Dressed qubit lifetime and coherence times

As the longitudinal decay time $T_{1\rho}$ in the driven frame is dependent on the noise of frequency Ω_R, it is often used for noise-spectroscopy measurements (see Ithier *et al.*[36], Yan *et al.*[37], Loretz *et al.*[38] and Supplementary Section 6). An example of a $T_{1\rho}$ measurement for $\Omega_R = 50$ kHz is shown in Fig. 4a. The decay curve yields $T_{1\rho}(50\text{ kHz}) = 1.3$ s. For higher Rabi frequencies, we observe a decrease in $T_{1\rho}$ (Supplementary Section 6 and Supplementary Fig. 4c).

To obtain $T_{2\rho}^{\star}$, we measure the free induction decay in two different ways. In Fig. 4b (upper panel) we look at the decay of the Rabi oscillations of the driven electron spin. This is equivalent to the free precession in the driven frame. The inset shows the actual Rabi oscillations, but we estimate the decay of the envelope from the main plot. The red lines correspond to an exponential decay $\propto e^{-(\tau/T_{2\rho}^{\star})^3}$, with $T_{2\rho}^{\star} = 2.4$ ms. In Fig. 4b (lower panel) we perform a Ramsey experiment in the driven frame. After the qubit is initialized in the $|+\rangle$ state, we use the standard pulse sequence $X_{\pi/2} - \tau - X_{\pi/2}$ (see inset) to measure the free induction decay. A slight detuning between ν_{RF} and Ω_R leads to the Ramsey fringes, which can be fitted with a decaying sinusoid (red lines) with $T_{2\rho}^{\star} = 2.4$ ms. We also measure the experimentally obtainable, low power-transition linewidth (Fig. 4c) of the dressed spin and obtain FWHM = 290 Hz for $P_{RF} = -26$ dBm (FWHM, full-width at half-maximum). This value is slightly above the intrinsic limit given by $T_{2\rho}^{\star}$, and is probably still limited by the excitation power.

The coherence time of the dressed qubit can be extended using dynamical decoupling, and in Fig. 4d we present the results of a Hahn echo, two-pulse Carr–Purcell–Meiboom–Gill (CPMG-2) and a four-pulse CPMG-4 sequence[39,40], performed with FM resonance (see above). We obtain $T_{2\rho}^{\text{Hahn}} = 9.2$ ms, $T_{2\rho}^{\text{CPMG-2}} = 17$ ms and $T_{2\rho}^{\text{CPMG-4}} = 23$ ms, respectively. Overall, the coherence times are one order of magnitude longer than those of the undriven spin[25], and are in line with similar measurements on MW-dressed atomic ions[7] and NV centres in diamond[11,41,42].

The improvement of the coherence times is achieved by the intrinsic insensitivity of the dressed states to magnetic field fluctuations. Dephasing is strongly suppressed as long as fluctuations in the background magnetic field are negligible compared with Ω_R, favouring the use of larger driving powers. However, higher B_1 amplitudes result in higher absolute B_1 fluctuations, which lowers $T_{2\rho}$. This can be circumvented by concatenated dressing of the states, in which power fluctuations of a first strong dressing field are mitigated by a second weaker dressing field[43]. Compared with pulsed dynamical decoupling sequences, continuous decoupling has three notable advantages. First, the dressed state is continuously protected from decoherence, whereas pulsed sequences only refocus the effects of a fluctuating background at specific times. Although it is known that gate operations can be interleaved within a pulsed dynamical decoupling sequence[44], the dressed qubit presents a more-flexible platform with which to perform an algorithm. Second, pulse errors in pulsed sequences can accumulate as the number of pulses is increased[45]. And third, pulsed sequences require much-higher pulse powers to obtain the same decoupling passband frequency[46]. This is because the role of Ω_R in the continuous scheme is played by the frequency at which pulses are applied in pulsed schemes.

Scalability

The use of the dressed spins as qubit states provides some interesting advantages for developing large-scale quantum-computation architectures[12,13]. Two of the four dressed qubit control mechanisms introduced above are compatible with scalable architectures based on a global always-on MW field and local gate operations[8,47]. This is because the dressed qubit can be controlled using local electric gates that apply an oscillating electric field (see above) or electric-field pulses (see above).

Coupling of two dressed qubits and the realization of two-qubit logic gates can be realized by spin–spin coupling via Hartmann–Hahn double resonance[4–6]. Considering two spins with slightly different hyperfine couplings caused by Stark or strain shifts, both can be dressed with MW fields resonant with their transition frequencies $\nu_{e1} \neq \nu_{e2}$, which creates dressed qubits with the level

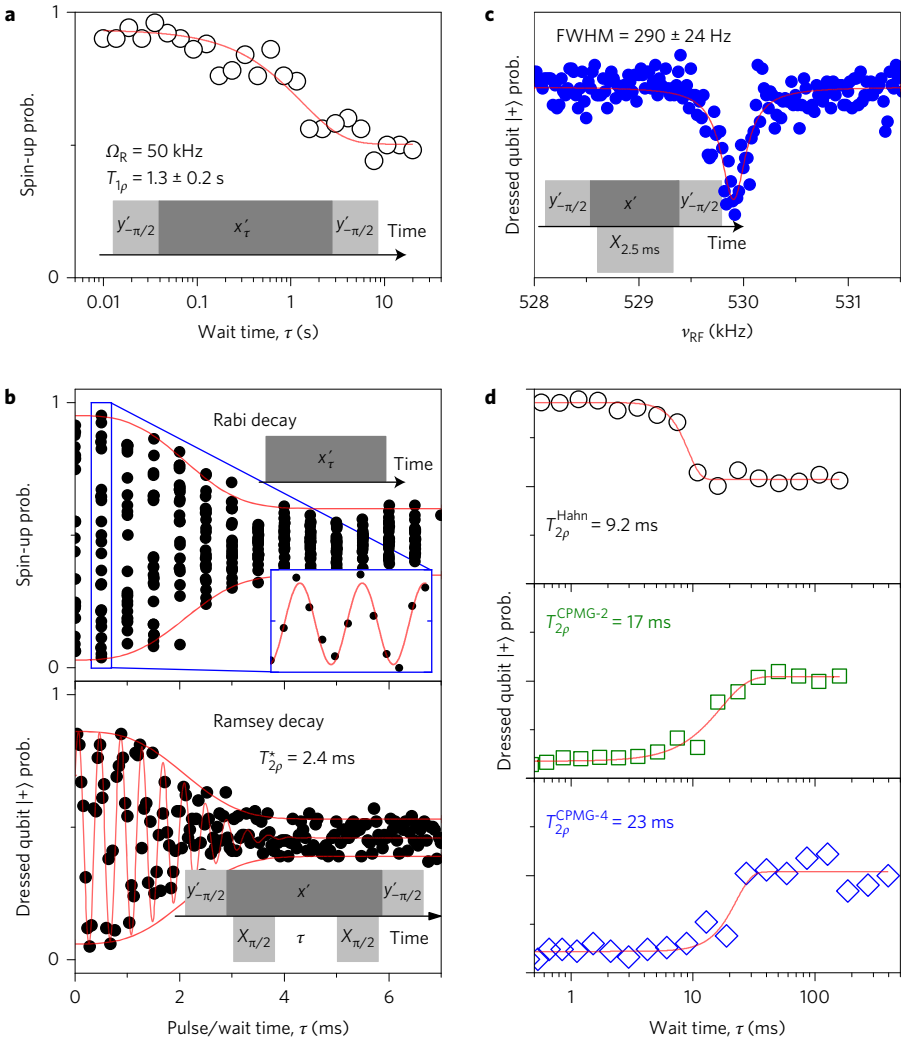

Figure 4 | Dressed qubit lifetime and coherence times. a, Longitudinal decay of the driven qubit $T_{1\rho}$. The inset shows the used pulse sequence. **b**, Free induction decay $T_{2\rho}^{*}$ of the dressed qubit obtained from (upper panel) the decay of the electron-spin Rabi oscillations measured at frequent intervals (the inset shows a zoom-in of the Rabi oscillations at around $\tau = 0.5$ ms) and (lower panel) a Ramsey sequence in the dressed frame using FM control (see insets for the pulse sequences). **c**, Low RF power, dressed qubit spectrum using FM control (see inset for the pulse sequence). **d**, Coherence times $T_{2\rho}^{Hahn}$, $T_{2\rho}^{CPMG-2}$ and $T_{2\rho}^{CPMG-4}$ obtained from Hahn echoes and CPMG sequences with two and four refocussing pulses using FM control, respectively.

splittings Ω_{R1} and Ω_{R2}, respectively. By choosing the two driving powers appropriately, the two dressed qubits can be tuned in resonance with each other ($\Omega_{R1} = \Omega_{R2}$) and coupled via exchange coupling or magnetic dipolar coupling[5]. Although smaller than exchange coupling for small distances, magnetic dipolar coupling decays more slowly, which makes it the dominant coupling mechanism for distances that exceed a few tens of nanometres. At a donor separation of 50 nm, a coupling strength of up to 400 Hz is achievable, and allows a number of gate operations to be conducted within the coherence time of the dressed qubit, assuming the use of dynamical decoupling. Furthermore, if a pair of quantum systems can be dressed by the same driving field, a hybrid dressed state can be created that is insensitive to both amplitude and phase noise in the continuous driving field[13].

Another interesting property that is enabled in the dressed basis is coupling of the spin states to strain in the crystal lattice[9], which could allow coherent qubit control by mechanical means[48,49], and the observation of coherent spin–phonon dynamics[50,51]. One could even envision coupling the dressed spins to micromechanical oscillators[10,11] and so realize long-distance spin–spin coupling via the quantized modes of the oscillator[52]. For this coupling scheme, a first MW field at ν_{MW1} would supply the dressing of the qubit with level splitting Ω_{R1}, and a local electric gate would control the dressed single-qubit rotations via an oscillating electric field. A d.c. electric field could then be used to Stark shift the spin transition into resonance with a second MW field at $\nu_{MW2} \neq \nu_{MW1}$ with strength $\Omega_{R2} \neq \Omega_{R1}$. This second MW drive would enable coupling to the micromechanical oscillator by bringing the dressed qubit into resonance with the oscillator's frequency at Ω_{R2}.

Summary and conclusions

In conclusion, our work demonstrates the encoding of quantum information in the dressed states of an electron spin on a phosphorus donor in silicon. We first prove the existence of dressed states by observing Mollow triplets in a pump–probe experiment and performing Rabi oscillations. We demonstrate four different control methods of the dressed qubit, of which two are compatible with scalable quantum-computing architectures; one results in faster gate operations than those obtainable with pulsed spin resonance on the bare electron spin and one achieves Rabi frequencies larger than the level splitting of the system. This variety of control methods is available because of the dressed basis, which also unlocks coupling to electric fields and lattice strain, and so opens promising avenues for future research and applications. Furthermore, we find coherence

times that are one order of magnitude longer than those of the bare spin, with $T_{2\rho}^{*} = 2.4$ ms and $T_{2\rho}^{\mathrm{Hahn}} = 9.2$ ms. Overall, this work provides a pathway to apply advanced control methods traditionally reserved for optical and atomic systems to a solid-state platform, which greatly expands the potential of spin qubits for applications in quantum-information processing and nanoscale research.

Received 19 March 2016; accepted 17 August 2016;
published online 17 October 2016

References

1. Mollow, B. R. Power spectrum of light scattered by two-level systems. *Phys. Rev.* **188,** 1969–1975 (1969).
2. Xu, X. *et al.* Coherent optical spectroscopy of a strongly driven quantum dot. *Science* **317,** 929–932 (2007).
3. Baur, M. *et al.* Measurement of Autler–Townes and Mollow transitions in a strongly driven superconducting qubit. *Phys. Rev. Lett.* **102,** 243602 (2009).
4. London, P. *et al.* Detecting and polarizing nuclear spins with double resonance on a single electron spin. *Phys. Rev. Lett.* **111,** 067601 (2013).
5. Hartmann, S. R. & Hahn, E. L. Nuclear double resonance in the rotating frame. *Phys. Rev.* **128,** 2042–2053 (1962).
6. Cai, J., Jelezko, F., Plenio, M. B. & Retzker, A. Diamond-based single-molecule magnetic resonance spectroscopy. *New J. Phys.* **15,** 013020 (2013).
7. Timoney, N. *et al.* Quantum gates and memory using microwave-dressed states. *Nature* **476,** 185–188 (2011).
8. Laucht, A. *et al.* Electrically controlling single-spin qubits in a continuous microwave field. *Sci. Adv.* **1,** 1500022 (2015).
9. Dreher, L. *et al.* Electroelastic hyperfine tuning of phosphorus donors in silicon. *Phys. Rev. Lett.* **106,** 037601 (2011).
10. Jonathan, D., Plenio, M. & Knight, P. Fast quantum gates for cold trapped ions. *Phys. Rev. A* **62,** 042307 (2000).
11. Rabl, P. *et al.* Strong magnetic coupling between an electronic spin qubit and a mechanical resonator. *Phys. Rev. B* **79,** 041302 (2009).
12. Mikelsons, G., Cohen, I., Retzker, A. & Plenio, M. B. Universal set of gates for microwave dressed-state quantum computing. *New J. Phys.* **17,** 053032 (2015).
13. Cai, J., Cohen, I., Retzker, A. & Plenio, M. B. Proposal for high-fidelity quantum simulation using a hybrid dressed state. *Phys. Rev. Lett.* **115,** 160504 (2015).
14. Pla, J. J. *et al.* A single-atom electron spin qubit in silicon. *Nature* **489,** 541–545 (2012).
15. Itoh, K. M. & Watanabe, H. Isotope engineering of silicon and diamond for quantum computing and sensing applications. *MRS Commun.* **4,** 143–157 (2014).
16. van Donkelaar, J. *et al.* Single atom devices by ion implantation. *J. Phys.* **27,** 154204 (2015).
17. Morello, A. *et al.* Architecture for high-sensitivity single-shot readout and control of the electron spin of individual donors in silicon. *Phys. Rev. B* **80,** 081307(R) (2009).
18. Morello, A. *et al.* Single-shot readout of an electron spin in silicon. *Nature* **467,** 687–691 (2010).
19. Dehollain, J. P. *et al.* Nanoscale broadband transmission lines for spin qubit control. *Nanotechnology* **24,** 015202 (2013).
20. Abragam, A. *The Principles of Nuclear Magnetism* Vol. 32 (Oxford Univ. Press, 1961).
21. Vandersypen, L. & Chuang, I. NMR techniques for quantum control and computation. *Rev. Modern Phys.* **76,** 1037–1069 (2005).
22. Jelezko, F. *et al.* Observation of coherent oscillation of a single nuclear spin and realization of a two-qubit conditional quantum gate. *Phys. Rev. Lett.* **93,** 130501 (2004).
23. Koppens, F. H. L. *et al.* Driven coherent oscillations of a single electron spin in a quantum dot. *Nature* **442,** 766–771 (2006).
24. Press, D., Ladd, T. D., Zhang, B. & Yamamoto, Y. Complete quantum control of a single quantum dot spin using ultrafast optical pulses. *Nature* **456,** 218–221 (2008).
25. Muhonen, J. T. *et al.* Storing quantum information for 30 seconds in a nanoelectronic device. *Nat. Nanotech.* **9,** 986–991 (2014).
26. Veldhorst, M. *et al.* An addressable quantum dot qubit with fault-tolerant control fidelity. *Nat. Nanotech.* **9,** 981–985 (2014).
27. Kroner, M. *et al.* Rabi splitting and ac-Stark shift of a charged exciton. *Appl. Phys. Lett.* **92,** 031108 (2008).
28. Wu, F. Y., Grove, R. E. & Ezekiel, S. Investigation of the spectrum of resonance fluorescence induced by a monochromatic field. *Phys. Rev. Lett.* **35,** 1426–1429 (1975).
29. Astafiev, O. *et al.* Resonance fluorescence of a single artificial atom. *Science* **327,** 840–843 (2010).
30. Jeschke, G. Coherent superposition of dressed spin states and pulse dressed electron spin resonance. *Chem. Phys. Lett.* **301,** 524–530 (1999).
31. Laucht, A. *et al.* Breaking the rotating wave approximation for a strongly-driven, dressed, single electron spin. Preprint at http://arxiv.org/1606.02380 (2016).
32. Nakamura, Y., Pashkin, Y. A. & Tsai, J. Coherent control of macroscopic quantum states in a single-Cooper-pair box. *Nature* **398,** 786–788 (1999).
33. DiVincenzo, D. P., Bacon, D., Kempe, J., Burkard, G. & Whaley, K. B. Universal quantum computation with the exchange interaction. *Nature* **408,** 339–342 (2000).
34. Petta, J. R. *et al.* Coherent manipulation of coupled electron spins in semiconductor quantum dots. *Science* **309,** 2180–2184 (2005).
35. Hanson, R. & Burkard, G. Universal set of quantum gates for double-dot spin qubits with fixed interdot coupling. *Phys. Rev. Lett.* **98,** 050502 (2007).
36. Ithier, G. *et al.* Decoherence in a superconducting quantum bit circuit. *Phys. Rev. B* **72,** 134519 (2005).
37. Yan, F. *et al.* Rotating-frame relaxation as a noise spectrum analyser of a superconducting qubit undergoing driven evolution. *Nature Commun.* **4,** 2337 (2013).
38. Loretz, M., Rosskopf, T. & Degen, C. Radio-frequency magnetometry using a single electron spin. *Phys. Rev. Lett.* **110,** 017602 (2013).
39. Hahn, E. L. Spin echoes. *Phys. Rev.* **80,** 580–594 (1950).
40. Meiboom, S. & Gill, D. Modified spin-echo method for measuring nuclear relaxation times. *Rev. Sci. Instrum.* **29,** 688–691 (1958).
41. Xu, X. *et al.* Coherence-protected quantum gate by continuous dynamical decoupling in diamond. *Phys. Rev. Lett.* **109,** 070502 (2012).
42. Golter, D. A., Baldwin, T. K. & Wang, H. Protecting a solid-state spin from decoherence using dressed spin states. *Phys. Rev. Lett.* **113,** 237601 (2014).
43. Cai, J. *et al.* Robust dynamical decoupling with concatenated continuous driving. *New J. Phys.* **14,** 113023 (2012).
44. Zhang, J., Souza, A. M., Brandao, F. D. & Suter, D. Protected quantum computing: interleaving gate operations with dynamical decoupling sequences. *Phys. Rev. Lett.* **112,** 050502 (2014).
45. Wang, Z.-H. *et al.* Effect of pulse error accumulation on dynamical decoupling of the electron spins of phosphorus donors in silicon. *Phys. Rev. B* **85,** 085206 (2012).
46. Álvarez, G. A. & Suter, D. Measuring the spectrum of colored noise by dynamical decoupling. *Phys. Rev. Lett.* **107,** 230501 (2011).
47. Kane, B. E. A silicon-based nuclear spin quantum computer. *Nature* **393,** 133–137 (1998).
48. Franke, D. P. *et al.* Interaction of strain and nuclear spins in silicon: quadrupolar effects on ionized donors. *Phys. Rev. Lett.* **115,** 057601 (2015).
49. Barfuss, A., Teissier, J., Neu, E., Nunnenkamp, A. & Maletinsky, P. Strong mechanical driving of a single electron spin. *Nat. Phys.* **11,** 820–824 (2015).
50. Soykal, O. O., Ruskov, R. & Tahan, C. Sound-based analogue of cavity quantum electrodynamics in silicon. *Phys. Rev. Lett.* **107,** 235502 (2011).
51. Gustafsson, M. V. *et al.* Propagating phonons coupled to an artificial atom. *Science* **346,** 207–211 (2014).
52. Bennett, S. D. *et al.* Phonon-induced spin–spin interactions in diamond nanostructures: application to spin squeezing. *Phys. Rev. Lett.* **110,** 156402 (2013).

Acknowledgements

This research was funded by the Australian Research Council Centre of Excellence for Quantum Computation and Communication Technology (project number CE110001027) and the US Army Research Office (W911NF-13-1-0024). We acknowledge support from the Australian National Fabrication Facility and from the laboratory of R. Elliman at the Australian National University for the ion-implantation facilities. The work at Keio was supported by the Japanese Society for the Promotion of Science JSPS KAKEN (S) and the Core-to-Core Program.

Author contributions

A.L., R.K., S.S., J.P.D., J.T.M., A.S.D. and A.M. designed the experiments. A.L. performed the measurements and analysed the results with A.M.'s supervision and R.K.'s and S.S.'s assistance. A.L. and F.A.M. performed the simulations with A.M.'s supervision. D.N.J. and J.C.M. designed and performed the ^{31}P implantation experiments. F.E.H. fabricated the device with A.S.D.'s supervision and R.K.'s and S.F.'s assistance. K.M.I. prepared and supplied the ^{28}Si epilayer wafer. A.L. and A.M. wrote the manuscript, with input from all the co-authors.

Additional information

Supplementary information is available in the online version of the paper. Reprints and permissions information is available online at www.nature.com/reprints. Correspondence and requests for materials should be addressed to A.L. and A.M.

Competing financial interests

The authors declare no competing financial interests.